CHEMISTRY OF MATERIALS
Article

Chem. Mater. **XXXX,** *XXX,* 000–000 A
DOI:10.1021/cm803218f

Strategies for Characterization of Large-Pore Metal-Organic Frameworks by Combined Experimental and Computational Methods

Youn-Sang Bae,[†] David Dubbeldam,[†] Andrew Nelson,[§] Krista S. Walton,[⊥] Joseph T. Hupp,[‡] and Randall Q. Snurr*[,†]

[†]*Department of Chemical and Biological Engineering, Northwestern University, 2145 Sheridan Road, Evanston, Illinois 60208,* [‡]*Department of Chemistry, Northwestern University, 2145 Sheridan Road, Evanston, Illinois 60208,* [§]*Naval Air Warfare Center, Weapons Division, China Lake, California 93555, and* [⊥]*Department of Chemical Engineering, Kansas State University, 1005 Durland Hall, Manhattan, Kansas 66506*

Received November 28, 2008. Revised Manuscript Received September 2, 2009

A large-pore IRMOF-16-like material (**1**) was synthesized solvothermally and evacuated by two solvent removal procedures: the original chloroform ($CHCl_3$) method and a new supercritical carbon dioxide (SCD) method. Using several experimental and geometric characterization tools, including thermogravimetric analysis (TGA), powder X-ray diffraction (PXRD), and pore size analysis, we propose that **1** is a mixture of noncatenated IRMOF-16 and the corresponding 2-fold interwoven structure and is partially collapsed during the evacuation, especially some of the larger pores. Adsorption measurements using several gases at 77 and 298 K showed that the new SCD evacuation is superior to the conventional $CHCl_3$ evacuation for increasing the adsorption kinetics as well as the adsorption capacity. This work illustrates a new strategy that combines several experimental methods, geometric calculations, and molecular simulations for the characterization of metal-organic frameworks (MOFs), especially those with large pores. This combination should be helpful for future characterization of new MOFs that possibly include some imperfections such as nonuniform catenation and partial collapse of the crystalline phase.

1. Introduction

Metal-organic frameworks (MOFs) have emerged recently as promising materials for separations, gas storage, catalysis, and chemical sensing.[1−4] For new MOFs, high-quality single crystals suitable for structural analysis are generally synthesized by slow reaction methods; however, for practical applications and for laboratory testing of adsorption properties, more rapid production may be desirable. Hence, faster solvothermal methods are applied for the synthesis of MOFs in larger quantities.[5,6] However, in some cases, the products synthesized via these methods have shown rather different properties, compared to highly crystalline MOF materials that have been prepared via slow reaction methods.[6] For example, studies of MOF-5, which is one of the most studied MOFs, have shown variations in the surface area in the range of 570−3800 m^2/g for materials synthesized by different procedures in different laboratories.[7−11] Recently, Hafizovic et al. used single-crystal X-ray diffraction and powder X-ray diffraction (PXRD), along with an array of other techniques, to analyze the differences in the surface areas of different MOF-5-like samples. They demonstrated that catenation of frameworks and the presence of organic and inorganic species in the micropores can greatly reduce the surface area.[6] Tsao et al. analyzed the large deviations in the surface areas of MOF-5-like materials using a combined small-angle X-ray scattering (SAXS) and wide-angle X-ray scattering (WAXS) analysis and found a fractal network of aggregated mesopores that reduce the surface area and hydrogen uptake at room temperature.[12] Kaye et al. obtained the highest reported surface area for MOF-5 by minimizing exposure to atmospheric or solvent water during sample preparation, and they argued that the differences in surface areas reported for MOF-5 could also be

*Author to whom correspondence should be addressed. E-mail: snurr@northwestern.edu.

(1) Mueller, U.; Schubert, M.; Teich, F.; Puetter, H.; Schierle-Arndt, K.; Pastre, J. *J. Mater. Chem.* **2006**, *16*, 626.
(2) Rowsell, J. L. C.; Yaghi, O. M. *Angew. Chem., Int. Ed.* **2005**, *44*, 4670.
(3) Snurr, R. Q.; Hupp, J. T.; Nguyen, S. T. *AIChE J.* **2004**, *50*, 1090.
(4) Férey, G. *Chem. Soc. Rev.* **2008**, *37*, 191.
(5) Rowsell, J. L. C.; Yaghi, O. M. *Microporous Mesoporous Mater.* **2004**, *73*, 3.
(6) Hafizovic, J.; Bjorgen, M.; Olsbye, U.; Dietzel, P. D. C.; Bordiga, S.; Prestipino, C.; Lamberti, C.; Lillerud, K. P. *J. Am. Chem. Soc.* **2007**, *129*, 3612.
(7) Eddaoudi, M.; Moler, D. B.; Li, H. L.; Chen, B. L.; Reineke, T. M.; O'Keeffe, M.; Yaghi, O. M. *Acc. Chem. Res.* **2001**, *34*, 319.
(8) Huang, L. M.; Wang, H. T.; Chen, J. X.; Wang, Z. B.; Sun, J. Y.; Zhao, D. Y.; Yan, Y. S. *Microporous Mesoporous Mater.* **2003**, *58*, 105.
(9) Panella, B.; Hirscher, M. *Adv. Mater.* **2005**, *17*, 538.
(10) Rowsell, J. L. C.; Millward, A. R.; Park, K. S.; Yaghi, O. M. *J. Am. Chem. Soc.* **2004**, *126*, 5666.
(11) Kaye, S. S.; Dailly, A.; Yaghi, O. M.; Long, J. R. *J. Am. Chem. Soc.* **2007**, *129*, 14176.
(12) Tsao, C. S.; Yu, M. S.; Chung, T. Y.; Wu, H. C.; Wang, C. Y.; Chang, K. S.; Chen, H. L. *J. Am. Chem. Soc.* **2007**, *129*, 15997.

explained by framework decomposition, because of exposure to water and humid air during and after the synthesis procedure.[11]

Because MOFs are crystalline, their surface areas can also be calculated geometrically from the corresponding crystal structures.[13] There are several ways to do this, and, in a recent study, Düren et al. recommended that the "accessible surface area" is more appropriate for assessing adsorption behavior than the often-used Connolly surface area.[14] Walton and Snurr simulated nitrogen isotherms in a series of MOFs and showed that the accessible surface areas agree very well with the Brunauer−Emmett−Teller (BET) surface areas obtained from the simulated isotherms.[15] This demonstrates that the surface areas obtained using the BET method are physically meaningful. It also suggests that comparing the geometrically calculated accessible surface area with the BET surface area obtained from an experimental N_2 adsorption isotherm can provide a useful characterization of deviations in the sample from the perfect crystal structure.[14,16] If the BET surface area is lower than the calculated accessible surface area, this could be due to the presence of reactants from the MOF synthesis, solvent molecules, partial collapse, or catenation.

One class of widely studied MOFs are the isoreticular MOFs (IRMOFs) discovered by Yaghi and co-workers.[17] This group includes MOF-5, which is also known as IRMOF-1. Although there have been many studies of IRMOF-1, IRMOF-3, IRMOF-6, and IRMOF-8, less is known about the gas adsorption characteristics of the IRMOFs with larger pores. There are especially few experimental studies of IRMOF-10, IRMOF-12, IRMOF-14, and IRMOF-16, which are the noncatenated counterparts of IRMOF-9, IRMOF-11, IRMOF-13, and IRMOF-15, respectively. This may be due to the difficulties in synthesizing these materials without catenation. Moreover, it can be quite difficult to effectively remove all of the solvent molecules (used in the synthesis procedure) from the pores of the large-pore MOFs without engendering either pore collapse or framework distortion.

Recently, we determined that the nitrogen-accessible surface areas of four representative MOFs could be very substantially enhanced by replacing a standard chloroform-exchange protocol with one that entails materials processing with liquid and supercritical carbon dioxide.[18] The improvements ranged from 1.6-fold to 12-fold. For at least some of the compounds examined, a major factor seems to be the ability of the supercritical drying (SCD) protocol to prevent the reversible collapse of interparticle mesopores, thereby forestalling blockage of the intraparticle micropores at particle/particle interfaces. Another significant component, however, may be prevention of the collapse of intraparticle micropores (i.e., crystallographically well-defined pores). In addition to our preliminary work on surface area enhancement in MOFs, we note an interesting recent report by Li et al. on the utility of SCD for removing residual solvent molecules.[19]

In the current study, one of the large-pore IRMOFs included in the preliminary report, an IRMOF-16-like material (denoted as **1**), was synthesized by a modification of the solvothermal method developed by Eddaoudi et al.[17] The main modification was the use of *N*,*N*′-dimethylformamide (DMF) in place of *N*,*N*′- diethylformamide (DEF). Once prepared, two solvent removal procedures were compared: the chloroform ($CHCl_3$) exchange method that was suggested by the Yaghi group and the new SCD method. We characterized these as-synthesized and evacuated materials using thermogravimetric analysis (TGA), powder X-ray diffraction (PXRD), and N_2 BET measurements (surface area, pore volume, and pore size distribution). These experimental results were then compared with geometrically calculated values from the perfect crystal structure of IRMOF-16 and several hypothetically catenated (2-fold and 3-fold interpenetrated and interwoven) structures. Furthermore, we compared the adsorption properties of CO_2, C_2H_6, CH_4, and H_2 at room temperature on **1** evacuated by $CHCl_3$ and SCD methods. In addition, these experimental isotherms were compared with grand canonical Monte Carlo (GCMC) simulations performed on the perfect crystal, as well as on several hypothetical catenated structures, to understand and interpret the experimental results. Finally, we computationally investigated the effect of guest solvents on the CO_2 isotherm at 298 K.

2. Experimental Methods

2.1. Synthesis. Commercial reagents were purchased from Sigma−Aldrich (ACS grade) and used as received unless otherwise noted. DMF was purified using a two-column solid-state purification system (Glasscontour System, Jeorg Meyer, Irvine, CA). Dehydrated 200-proof (≥99.5%) absolute ethanol was used as received. An IRMOF-16-like sample (**1**) was prepared by a modification of the solvothermal method developed by Eddaoudi et al.[17] $Zn(NO_3)_2 \cdot 6H_2O$ (1.01 g, 3.4 mmol) and the acid form of terphenyl-2,2′-dicarboxylate (TPDC) (0.270 g, 0.848 mmol) were mixed in 1200 mL of DMF, which was used in place of DEF. Here, note that a diluted solution was used, because the solubility of TPDC in DMF is extremely low. The 1200-mL solution was equally partitioned between 4 1-L bottles that were sealed and heated at 100 °C for 48 h. The resulting crystals were filtered and washed with 2 L of DMF, paying careful attention to keep the crystals wet with solvent at all times, and then were stored under fresh DMF prior to being evacuated.

2.2. Characterization. Powder X-ray diffraction (PXRD) patterns were recorded with a Rigaku Model XDS 2000

(13) Leach, A. R. *Molecular Modelling: Principles and Applications*, 2nd ed.; Prentice Hall: Harlow, England, 2001.
(14) Düren, T.; Millange, F.; Férey, G.; Walton, K. S.; Snurr, R. Q. *J. Phys. Chem. C* **2007**, *111*, 15350.
(15) Walton, K. S.; Snurr, R. Q. *J. Am. Chem. Soc.* **2007**, *129*, 8552.
(16) Liu, J.; Culp, J. T.; Natesakhawat, S.; Bockrath, B. C.; Zande, B.; Sankar, S. G.; Garberoglio, G.; Johnson, J. K. *J. Phys. Chem. C* **2007**, *111*, 9305.
(17) Eddaoudi, M.; Kim, J.; Rosi, N.; Vodak, D.; Wachter, J.; O'Keeffe, M.; Yaghi, O. M. *Science* **2002**, *295*, 469.
(18) Nelson, A. P.; Farha, O. K.; Mulfort, K. L.; Hupp, J. T. *J. Am. Chem. Soc.* **2009**, *131*, 458.
(19) Li, K.; Olson, D. H.; Lee, J. Y.; Wenhua, B.; Wu, K.; Yuen, T.; Xu, Q.; Li, J. *Adv. Funct. Mater.* **2008**, *18*, 2205.

diffractometer using nickel-filtered Cu Kα radiation (λ = 1.5418 Å) over a range of $5° < 2\theta < 40°$ in 0.1° steps with a counting time per step of 1 s. Powder samples were placed in a diffractometer that was mounted on a stainless steel holder with double-sided tape. TGA was performed on a Mettler−Toledo Model TGA/SDTA851e device. Samples (3−5 mg) in alumina pans were heated from 25 to 700 at 10 °C/min under N_2 atmosphere. Nitrogen adsorption isotherms were measured with an Autosorb 1-MP from Quantachrome Instruments. Samples of a known weight (35−50 mg) were loaded into a sample tube and evacuated under 10^{-5} torr dynamic vacuum at room temperature for 24 h. After evacuation, the sample and tube were precisely weighed again to obtain the evacuated sample weight.

2.3. Solvent Removal Method. To remove guest solvent molecules from the frameworks, two evacuation procedures were compared. The first procedure followed the chloroform ($CHCl_3$) exchange method that was developed by the Yaghi group.[17,20] The as-synthesized crystals were washed with $CHCl_3$ to remove the DMF from the surface, and then they were immersed in $CHCl_3$ and allowed to soak for 3 d. During this time, the soaking solution was replaced with fresh $CHCl_3$ every 24 h. After the solvent exchange process was completed, the sample was filtered, dried in air for 30 min, and placed under vacuum at room temperature for 24 h. The second evacuation method was the new SCD method that was developed at Northwestern.[18] The as-synthesized crystals were soaked in ethanol for 3 d to exchange all the guest solvents with ethanol. Again, the soaking solution was replaced with new ethanol every 24 h. The ethanol-exchanged samples were then soaked in liquid CO_2 in a supercritical dryer for more than 6 h, purging the chamber with fresh liquid CO_2 every hour. During this period, the temperature in the dryer was maintained between −5 °C to +5 °C. The temperature was then increased to 40 °C (i.e., above the critical point of CO_2 (31 °C)) and maintained for 30 min. Finally, the supercritical CO_2 in the drying chamber was slowly released over 18 h. We tried to handle the samples carefully, to prevent degradation from water adsorption. During the solvent exchanges using $CHCl_3$ or ethanol, the MOF samples were kept wet at all times to prevent water adsorption. At all times except gas adsorption, the evacuated samples were placed in sealed containers and stored in a desiccator.

2.4. Adsorption Measurement. The adsorption isotherms of CO_2, CH_4, C_2H_6, and H_2 on samples evacuated by either $CHCl_3$ or SCD methods were measured volumetrically at 298 K, up to pressures of 18 atm. Before each measurement, the sample was placed under vacuum overnight in the adsorption chamber, and the void volume of the system was determined using helium gas. CO_2 (99.9%), CH_4 (99%), C_2H_6 (99%), and H_2 (99.999%) were obtained from Airgas, Inc. (Radnor, PA). Prior to analysis, gas was passed through a zeolite trap to remove residual moisture. Adsorbate was dosed into the system incrementally and equilibrium was assumed when no further change in pressure was observed (within 0.01 kPa). The excess adsorbed amounts per unit adsorbent mass were calculated by a mass balance for the pure gas in the injection and sample sides using the generalized virial-coefficient equation of state (see the Supporting Information). The detailed procedure can be found elsewhere.[21]

3. Simulations

The noncatenated IRMOF-16 framework structure was taken from the crystallographic unit cell.[17] Several hypothetical catenated frameworks were generated on the computer by copying atoms of the original IRMOF-16 framework and translating these positions along the [111] direction. Theoretically, two more frameworks can be added into the large pore space of the original IRMOF-16 (noncatenated) without atomic overlap. Hence, we generated 2-fold and 3-fold catenated variations of IRMOF-16. For catenation, we can define two different configurations: interwoven and interpenetrated. The 2-fold and 3-fold *interwoven* configurations were generated by minimizing the distances between two or three frameworks without atomic overlap. (In these structures, the second and the third frameworks are shifted 26% and 52% of the cavity length along the [111] direction.) The *interpenetrated* configurations were generated by maximizing these distances.[22] In the 2-fold interpenetrated structure, the second framework is shifted exactly one-half of the cavity length in the *x*-, *y*-, and *z*-directions. In the 3-fold interpenetrated structure, the second and third frameworks are shifted one-third and two-thirds of the cavity length, respectively. (See Figure S1 in the Supporting Information.)

The accessible surface areas and total pore volumes of the original IRMOF-16 and hypothetical catenated structures were calculated in a geometric fashion using a simple Monte Carlo integration technique.[14,15] Nitrogen-sized (3.72 Å) and zero-sized (0 Å) probes were used for the calculations of the accessible surface area and the total pore volume, respectively. The simulated PXRD patterns were calculated over a range of $1° < 2\theta < 40°$ in 0.1° steps, using the Materials Studio software (version 4.0). The geometric pore size distributions were calculated according to the method of Gelb and Gubbins.[23]

Simulated adsorption isotherms for the IRMOF-16 and hypothetical catenated structures were obtained using the GCMC algorithm.[24,25] The volume (V), the temperature (T), and the chemical potential (μ) are kept fixed, and, under these conditions, the average number of molecules is computed. Framework flexibility was ignored, and positions of the frameworks were fixed. However, for the simulations in catenated structures with guest solvent molecules (DMF or water), the frameworks were allowed to move relative to each other. Framework−framework interactions consisted of Lennard-Jones interactions with parameters from the DREIDING model[26] and Coulombic interactions due to partial charges placed on all framework atoms. The partial

(20) Eddaoudi, M.; Li, H. L.; Yaghi, O. M. *J. Am. Chem. Soc.* **2000**, *122*, 1391.
(21) Bae, Y.-S.; Mulfort, K. L.; Frost, H.; Ryan, P.; Punnathanam, S.; Broadbelt, L. J.; Hupp, J. T.; Snurr, R. Q. *Langmuir* **2008**, *24*, 8592.
(22) Ryan, P.; Broadbelt, L. J.; Snurr, R. Q. *Chem. Commun.* **2008**, 4132.
(23) Gelb, L. D.; Gubbins, K. E. *Langmuir* **1999**, *15*, 305.
(24) Allen, M. P.; Tildesley, D. J. *Computer Simulation of Liquids*; Oxford Science Publications: New York, 1987.
(25) Frenkel, D.; Smit, B. *Understanding Molecular Simulation from Algorithms to Applications*; Academic Press: San Diego, CA, 2002.
(26) Mayo, S. L.; Olafson, B. D.; Goddard, W. A. *J. Phys. Chem.* **1990**, *94*, 8897.

charges were calculated with the CHELPG method provided in the Gaussian03 program,[27] following DFT calculations with the PBEPBE density functional[28] and a 6-31G* basis set. The same method was previously applied for the charge calculation in IRMOF-1.[29] Lennard-Jones potentials were shifted to zero at the cutoff of 12 Å. The parameters for methane, ethane, and CO_2 were taken from the TraPPE model,[30,31] and the parameters for hydrogen were obtained from a three-point model.[32] Cross-interaction parameters with the framework were computed using Lorentz−Berthelot mixing rules. In previous work,[33] this force field was shown to predict adsorption of CO_2 and methane in IRMOF-1, in good agreement with the experiment. Some adsorption isotherms were obtained with guest solvent molecules water (Tip5p-EW model)[34] and DMF (CS2 model)[35] in the MOF at a fixed loading of solvent. The water and DMF molecules were considered to be rigid. Monte Carlo (MC) moves for the solvent molecules were translation, rotation, and random reinsertion. The adsorbates themselves have additional MC moves of random insertion from and deletion to an imaginary reservoir of particles kept at the appropriate pressure and temperature. All isotherms used at least 100 000 cycles for the production run (after equilibration), where 1 cycle is defined as one MC move per molecule (on average). Because molecular simulation predicts the absolute number of sorbate molecules within the MOF under the given gas-phase conditions, the excess adsorption was determined from the absolute adsorption, using the procedure described previously.[36] All adsorption results are given in terms of excess adsorption, unless otherwise noted. The detailed potentials parameters used in the GCMC simulations are shown in the Supporting Information.

(27) Frisch, M. J.; Trucks, G. W.; Schlege, l. H. B.; Scuseria, G. E.; Robb, M. A.; Cheeseman, J. R.; Montgomery, J., J. A.; Vreven, T.; Kudin, K. N.; Burant, J. C.; Millam, J. M.; Iyengar, S. S.; Tomasi, J.; Barone, V.; Mennucci, B.; Cossi, M.; Scalmani, G.; Rega, N.; Petersson, G. A.; Nakatsuji, H.; Hada, M.; Ehara, M.; Toyota, K.; Fukuda, R.; Hasegawa, J.; Ishida, M.; Nakajima, T.; Honda, Y.; Kitao, O.; Nakai, H.; Klene, M.; Li, X.; Knox, J. E.; Hratchian, H. P.; Cross, J. B.; Adamo, C.; Jaramillo, J.; Gomperts, R.; Stratmann, R. E.; Yazyev, O.; Austin, A. J.; Cammi, R.; Pomelli, C.; Ochterski, J. W.; Ayala, P. Y.; Morokuma, K.; Voth, G. A.; Salvador, P.; Dannenberg, J. J.; Zakrzewski, V. G.; Dapprich, S.; Daniels, A. D.; Strain, M. C.; Farkas, O.; Malick, D. K.; Rabuck, A. D.; Raghavachari, K.; Foresman, J. B.; Ortiz, J. V.; Cui, Q.; Baboul, A. G.; Clifford, S.; Cioslowski, J.; Stefanov, B. B.; Liu, G.; Liashenko, A.; Piskorz, P.; Komaromi, I.; Martin, R. L.; Fox, D. J.; Keith, T.; Al-Laham, M. A.; Peng, C. Y.;Nanayakkara, A.; Challacombe, M.; Gill, P. M. W.; Johnson, B.; Chen, W.; Wong, M. W.; Gonzalez, C.; Pople, J. A. *Gaussian 03, Revision C.02*; Gaussian, Inc.: Wallingford, CT, 2004.
(28) Perdew, J. P.; Burke, K.; Ernzerhof, M. *Phys. Rev. Lett.* **1996**, *77*, 3865.
(29) Sagara, T.; Klassen, J.; Ganz, E. *J. Chem. Phys.* **2004**, *121*, 12543.
(30) Martin, M. G.; Thompson, A. P.; Nenoff, T. M. *J. Chem. Phys.* **2001**, *114*, 7174.
(31) Potoff, J. J.; Siepmann, J. I. *AIChE J.* **2001**, *47*, 1676.
(32) Dakrim, F.; Levesque, D. *J. Chem. Phys.* **1998**, *109*, 4981.
(33) Dubbeldam, D.; Walton, K. S.; Ellis, D. E.; Snurr, R. Q. *Angew. Chem., Int. Ed.* **2007**, *46*, 4496.
(34) Rick, S. W. *J. Chem. Phys.* **2004**, *120*, 6085.
(35) Chalaris, M.; Samios, J. *J. Chem. Phys.* **2000**, *112*, 8581.
(36) Frost, H.; Düren, T.; Snurr, R. Q. *J. Phys. Chem. B* **2006**, *110*, 9565.

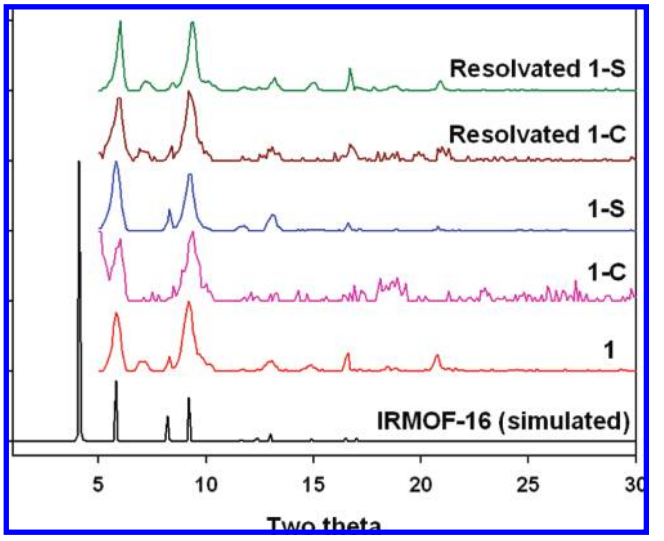

Figure 1. PXRD patterns for as-synthesized (**1**), evacuated (**1-C** and **1-S**), and resolvated samples, together with the simulated pattern for IRMOF-16.

4. Results and Discussion

4.1. Characterization by Experimental and Geometric Methods. Figure 1 shows the experimental PXRD patterns of an as-synthesized sample (denoted as **1**), samples evacuated by $CHCl_3$ (denoted as **1-C**) or SCD methods (denoted as **1-S**), and samples resolvated by DMF after the evacuations. These are compared with the simulated PXRD pattern of an original IRMOF-16 crystal.[17] As shown in the figure, the peak positions of **1** are in general agreement with the simulated pattern of IRMOF-16. A peak at 4° is shown in the simulated pattern but could not be observed in the experimental patterns, because 5° was the lowest 2θ value that our machine could measure.

In the case of the $CHCl_3$ evacuation (**1-C** sample), the signal-to-noise ratio is worse and a new peak is observed at a low 2θ angle (5°). This may be due to the weak crystallinity originating from the $CHCl_3$ evacuation. When **1-C** is resolvated in DMF, the peak at 5° disappears and peak intensities were slightly recovered. This can possibly be explained by a change in the framework structure, depending on the nature of the occluded solvent (DMF or chloroform). Similar reversible dynamic behavior has been reported in many MOFs. (See ref 21 and references cited therein.) However, when **1** is evacuated via the SCD method (**1-S** sample), only minor changes are observed in the PXRD pattern. Here, it is noteworthy that the relative intensities of the reflections at low angles (5.8° and 8.2°) become slightly stronger, compared to those of **1**. Moreover, for the case of **1-S**, the relative peak intensities of PXRD pattern are similar to those observed in the simulated PXRD pattern for IRMOF-16; however, the PXRD patterns for **1-C** do not show this coincidence. This may be because considerable guest DMF molecules are still in the pores of **1-C** while most of them have been removed from the pores of **1-S**. Also, both the positions and intensities of all peaks observed in **1** are recovered after the resolvation of **1-S**.

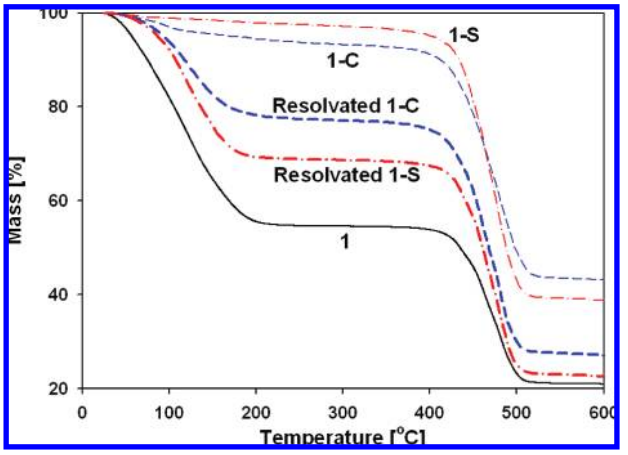

Figure 2. TGA results for as-synthesized (**1**), evacuated (**1-C** and **1-S**), and resolvated samples.

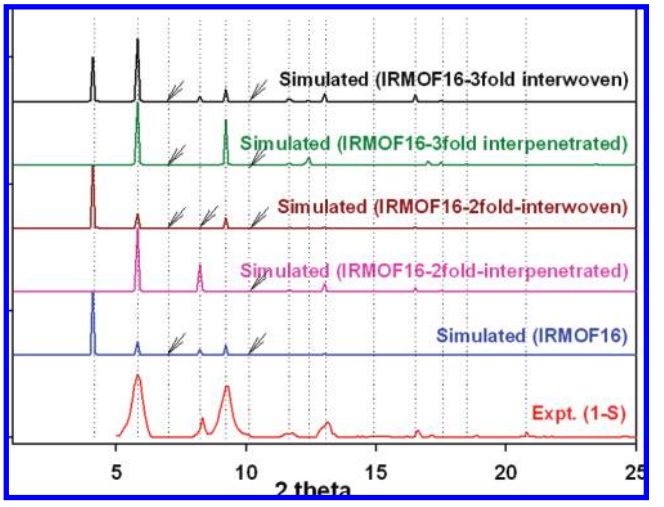

Figure 3. Comparison of the experimental PXRD pattern for **1-S** with the simulated patterns for original IRMOF-16 and several hypothetical catenated structures. Arrows indicate minor peaks.

These results indicate that the new SCD method is superior to the conventional $CHCl_3$ method for the evacuation of **1**. On the other hand, the peaks at 7.1°, 12.4°, and 14.9° are not visible after **1** is evacuated by the SCD method (**1-S**), but these peaks are recovered when **1-S** is resolvated. This could be due to the flexible movements of organic struts as the guest solvents are removed from the MOF cavities.

Figure 2 shows the TGA results for the as-synthesized sample (**1**), evacuated samples (**1-C** and **1-S**), and resolvated samples. All of the TGA curves indicate thermal stability of the framework up to 400 °C, where decomposition of the framework starts. For the TGA curve of **1**, the initial mass loss between 25 and 400 °C (46 wt %), corresponding to the removal of guest solvents, is smaller than the theoretical mass percentage of solvent (59 wt %) in the original crystal structure of IRMOF-16. This indicates that **1** has a smaller pore volume than the perfect crystal. Hafizovic et al. reported that the pure MOF-5 phase is difficult to synthesize without catenation or the presence of nonvolatile reactants in the pores.[6] Therefore, it is possible that **1** exists as a catenated version of IRMOF-16. However, IRMOF-15, a 2-fold interpenetrated form of IRMOF-16 for which the structure is known,[17] has a much smaller theoretical mass percentage of solvents (13 wt %) than that in **1** (46 wt %). Considering the pore volumes (see Table 2, presented later in this work), 2-fold interpenetrated and interwoven structures should have similar mass percentages of solvent as IRMOF-15. In a similar way, 3-fold interpenetrated and interwoven structures should have even smaller values than IRMOF-15. Hence, neither a pure phase of a catenated structure nor a mixed phase of several catenated structures can produce the 46 wt % solvent loss observed in the TGA curve of **1**. Such a large solvent loss can be obtained only if **1** contains (at least partially) a phase with large pore volume, such as the noncatenated IRMOF-16. This suggests that **1** may be a mixture of noncatenated and catenated versions of IRMOF-16. In this study, we devised a combined characterization method including several experimental measurements and geometric calculations to support this hypothesis. These will be discussed in greater detail below.

The TGA curves of the evacuated samples (**1-C** and **1-S**) show that some amount of solvent remains in the pores after evacuation, which indicates that neither method is perfect for the complete evacuation of **1**. Nevertheless, the solvent molecules remaining in **1-S** (3.5 wt %) amount to only half of those left in **1-C** (7.3 wt %). After resolvation, the samples previously evacuated by $CHCl_3$ and SCD methods contain 23 and 32 wt % solvents, respectively. These are only ~50% and 70%, compared to that of the as-synthesized sample (**1**). This shows that pore volume of **1** becomes irreversibly contracted after both evacuation procedures. These pore volume reductions may come from partial collapse or distortion of frameworks during the evacuations, which is an additional consequence of the large pore sizes of IRMOF-16.

To further test the hypothesis that **1** is a mixture of noncatenated and catenated frameworks of IRMOF-16, we performed several experimental and geometric characterizations for the original IRMOF-16 framework, in addition to several hypothetical, catenated frameworks. Figure 3 compares the experimental PXRD pattern of **1-S** with the simulated patterns of original IRMOF-16, 2-fold and 3-fold interpenetrated structures, as well as 2-fold and 3-fold interwoven structures. The peak positions of **1-S** are consistent with simulated patterns of IRMOF-16, although the peak at 4° could not be observed because of the limitations of our machine. In the PXRD patterns of 2-fold and 3-fold interwoven frameworks, all the peaks observed in the PXRD pattern of the original IRMOF-16 can be found. However, in the PXRD patterns of 2-fold and 3-fold interpenetrated frameworks, some of the peaks are missing (peaks at 4.0°, 7.1°, 9.1°, and 12.4° for 2-fold interpenetrated structure, and peaks at 4.0°, 8.2°, and 13.1° for 3-fold interpenetrated structure), although the other peaks are observed in the same positions as those of the original

Table 1. Comparison between Pore Diameters Obtained from Experimental N_2 Isotherms and Geometric Calculations

compound	pore diameters (Å)												
						Experiment[a]							
1-C		4.4		4.9	5.4	6.0		8.6		10.5		11.7	
1-S		4.4		4.9		6.0		8.6		10.5		11.5	
						Calculated							
IRMOF-16													23.6
2-interpenetrated							7.4	8.6	9.6		11.2		
2-interwoven		4.4				6.0		8.5		10.5		11.7	12.5/12.9/14.2/14.8
3-interpenetrated	3.8/4.2		4.7	5.0		5.9	7.3/8.2						
3-interwoven	3.5				5.3		6.7	8.9		10.7			
IRMOF-15							7.4		9.6				

[a] Experimental pore diameters were obtained by H−K method from N_2 isotherms at 77 K.

Table 2. Surface Areas and Pore Volumes from Experimental Measurements and Geometric Calculations

	surface area (m^2/g)	total pore volume (cm^3/g)
	Experimental Measurements[a,b]	
1-C	472	0.233
1-S	1912	0.816
	Geometric Calculations[c]	
IRMOF-16	6225	4.485
2-interpenetrated	6195	1.972
2-interwoven	3851	1.972
3-interpenetrated	3012	1.161
3-interwoven	2993	1.161
IRMOF-15	6074	1.960

[a] Experimental surface areas were measured via the BET method from N_2 isotherms at 77 K ($0.01 < P/P_0 < 0.1$). [b] Experimental total pore volumes were calculated for pores < 36 Å in size (at $P/P_0 = 0.45$) from the N_2 isotherm at 77 K. [c] Accessible surface areas were calculated geometrically using a simple Monte Carlo integration technique with full details given previously.[14]

IRMOF-16. Because all the PXRD peaks in catenated frameworks overlap with those in the original noncatenated framework, it is difficult to determine based on PXRD alone if **1** is a pure phase of original IRMOF-16, one of the interwoven frameworks, or a mixture of noncatenated and catenated versions of IRMOF-16. However, at least this result does not contradict our suggestion that **1** is a mixture of noncatenated and catenated frameworks of IRMOF-16.

Table 1 compares the peaks in the pore size distributions from experimental N_2 isotherms for evacuated samples with those from geometric calculations for the original IRMOF-16 and several hypothetical catenated frameworks. The experimental pore size distributions were obtained using the Horvath−Kawazoe (H−K) method, based on slit-shape pore geometry.[37] As shown in Table 1, the pore size distributions experimentally measured for both evacuated samples (**1-C** and **1-S**) are similar with each other and show much smaller pores than the original IRMOF-16 (23.6 Å). Also, they are very different from the geometric pore size distributions for 2-fold interpenetrated, 3-fold interpenetrated, 3-fold interwoven, and IRMOF-15 structures. Interestingly, the peaks for the 2-fold interwoven structure almost match with the results for **1-C** and **1-S**. The 2-fold interwoven framework has pores of 4.4, 6.0, 8.5, 10.5, and 11.7 Å, which were also observed in **1-C** and **1-S**. (See the Supporting Information.) However, large pores in the 2-fold interwoven structure (12.5, 12.9, 14.2, and 14.8 Å) were not observed in **1-C** and **1-S**. The collapse of these large pores during the evacuation procedures is one possible explanation, and the pores of 4.9 and 5.4 Å in the evacuated samples (**1-C** and **1-S**) may be the result of pore collapse. Also, it is possible that the missing large pores are a result of unremoved guest solvent molecules (DMF and/or H_2O).

Note that the H−K method has well-known limitations.[38] It assumes a simple pore geometry (slit pore, cylindrical, or spherical) and particular surface properties. It can also be sensitive to the quality of the experimental data. In addition, it only applies to micropores but not mesopores. Methods based on density functional theory (DFT) are now acknowledged to be superior for obtaining pore size distributions from adsorption data. Unfortunately, the necessary kernels for DFT calculations in MOFs are not available. Therefore, we, and others, have used the H−K method for MOFs,[39−41] but we must interpret the results cautiously. The results in Table 1 can only suggest that **1** has a 2-fold interwoven structure in it. Further support is provided by the other techniques discussed in this paper.

Table 2 compares the surface areas and total pore volumes of experimental evacuated samples (**1-C** and **1-S**) with those calculated for original IRMOF-16 and the hypothetical catenated frameworks. As shown in this table, **1-S** has a much larger surface area and pore volume than **1-C** does. However, even **1-S** has a much smaller surface area and pore volume than that of the original IRMOF-16 structure. Similar discrepancies between the experimental and calculated surface area were already observed in other large-pore IRMOFs, IRMOF-12, and IRMOF-14.[14,15,17] Moreover, the surface area and pore volume of **1-S** are considerably smaller than those of the

(37) Horvath, G.; Kawazoe, K. *J. Chem. Eng. Jpn.* **1983**, *16*, 470.
(38) Thommes, M. Textual Characterization of Zeolites and Ordered Mesoporous Materials by Physical Adsorption. In *Introduction to Zeolite Science and Practice*, 3rd Revised Edition; Cejka, J., van Bekkum, H., Corma, A., Schüth, F., Eds.; Elsevier B.V.: Amsterdam, 2007.
(39) Wang, Z.; Tanabe, K. K.; Cohen, S. M. *Inorg. Chem.* **2009**, *48*, 296.
(40) Makhseed, S.; Samuel, J. *Chem. Commun.* **2008**, 4342.
(41) Farha, O. K.; Spokoyny, A. M.; Mulfort, K. L.; Hawthorne, M. F.; Mirkin, C. A.; Hupp, J. T. *J. Am. Chem. Soc.* **2007**, *129*, 12680.

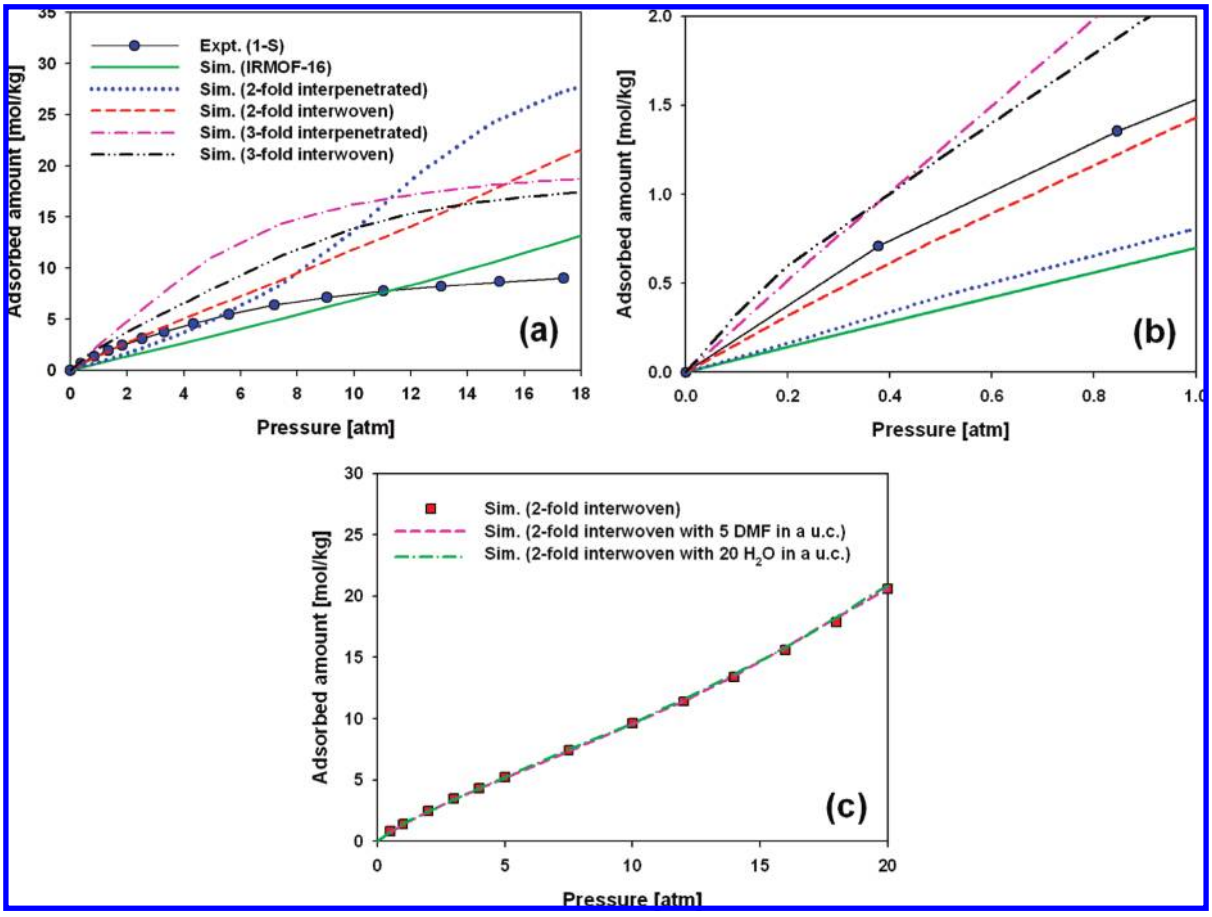

Figure 4. (a) Comparison of experimental CO_2 isotherm in **1-S** with those in IRMOF-16 and several hypothetical catenated structures at 298 K, (b) low-pressure region of the isotherms, and (c) comparison of simulated CO_2 isotherms in the hypothetical 2-fold interwoven structure with and without solvent molecules at 298 K. Note that the simulated isotherms in panel c are presented in terms of absolute adsorption and were obtained by simulations that allowed the frameworks to move relative to each other.

hypothetical 2-fold interwoven structure. This may also be due to the partial collapse after the evacuation and/or some remaining guest solvents, as mentioned previously.

4.2. Effects of Catenation and Guest Solvents on CO_2 Adsorption. To see the effect of catenation on gas adsorption isotherms, we performed GCMC simulations for CO_2 adsorption in hypothetical 2-fold and 3-fold interpenetrated and interwoven structures at 298 K. We then compared these to the CO_2 isotherm of **1-S** measured experimentally at 298 K. Figures 4a and 4b illustrate this comparison. At low pressures, the order of the isotherm slope is as follows:

$$\begin{aligned}\text{original IRMOF-16} &< \text{2-fold interpenetrated}\\ &< \text{2-fold interwoven} \approx \textbf{1-S}\\ &< \text{3-fold interpenetrated}\\ &< \text{3-fold interwoven}\end{aligned}$$

As expected, this order coincides with the order of the smallest pore of each structure (see Table 1), and the large-pore IRMOF-16 shows the weakest adsorption. The 2-fold interwoven structure shows a slightly steeper isotherm than the 2-fold interpenetrated structure, because it has small pockets (4.4 and 6.0 Å, as reported in Table 1), where CO_2 molecules can interact with two metal corner sites simultaneously. In the intermediate pressures, however, the interwoven structure shows smaller adsorbed amounts than the interpenetrated structure, because the main pores of the interwoven structure (11.7 and 14.2 Å) are larger than those of the interpenetrated one (9.6 and 11.2 Å). At the saturation region, both the interpenetrated and interwoven structures give similar adsorption (~30 mol/kg), because of the similar pore volumes (see Table 2). These are considerably larger than the experimental isotherm, and this is consistent with the surface areas and pore volumes reported in Table 2. Similar behaviors are observed for the 3-fold interpenetrated and interwoven structures: at very low pressures, the 3-fold interwoven structure shows a slightly steeper isotherm; in the intermediate pressures, the 3-fold interpenetrated structure shows larger adsorbed amounts; at the saturation region, the adsorbed amounts of both structures converge. It is interesting to note that, at low pressures (< 5 atm), the experimental isotherm for **1-S** matches very well with the simulated isotherm for the 2-fold interwoven structure. This can be explained by the similar pore sizes, especially for small pores (4.0 and 6.0 Å). This supports the hypothesis that **1** contains a 2-fold interwoven structure.

To investigate the effect of the guest solvents on the gas adsorption, we did several GCMC simulations for CO_2

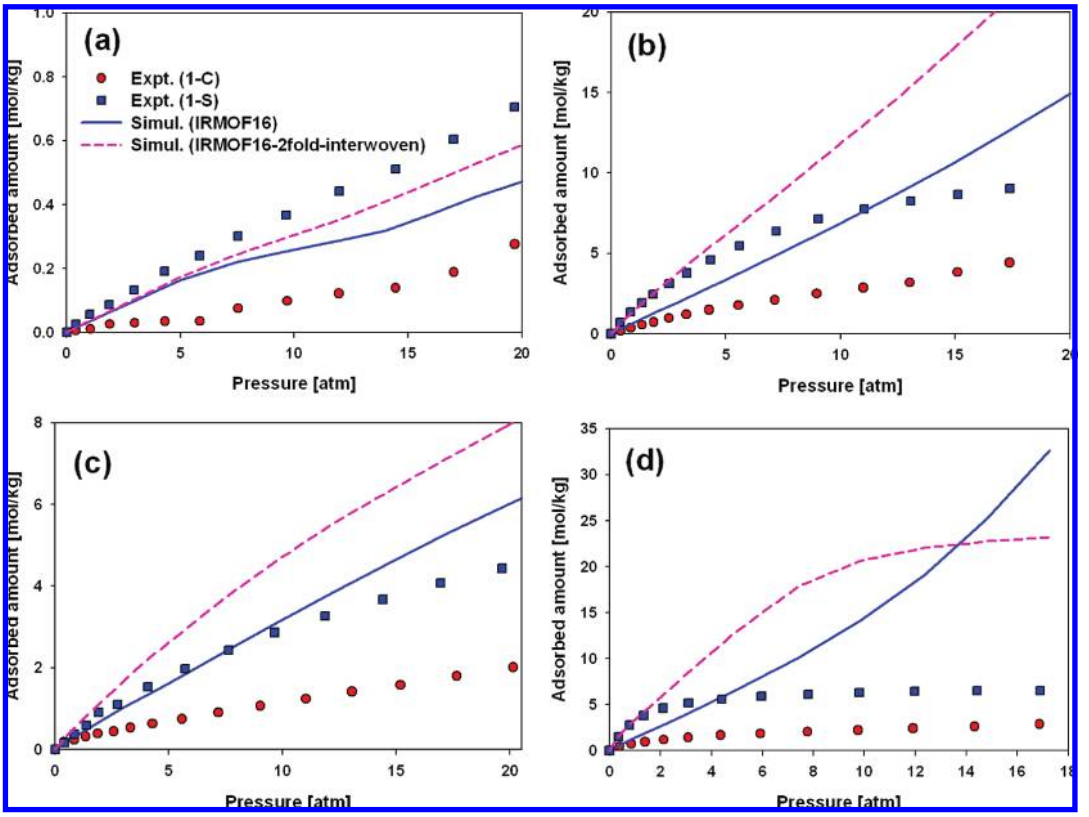

Figure 5. Comparisons between the experimental isotherms for **1-C** and **1-S** and the simulated isotherms for IRMOF-16 and 2-fold interwoven structures at 298 K: (a) H_2, (b) CO_2, (c) CH_4, and (d) C_2H_6.

adsorption in the hypothetical 2-fold interwoven structure containing some guest solvents in the pores. For these simulations, the frameworks were allowed to move relative to each other during the CO_2 adsorption. However, we observed no loading-induced framework movements, because of the strength of the framework−framework interaction, compared to the framework−adsorbate interactions. The fluctuations in the framework−framework distance were smaller than half an angstrom and independent of CO_2 loading and solvent molecules (H_2O and DMF). From the TGA results, we can argue that ~3.5 wt % of the solvents remain in **1-S** following evacuation. This corresponds to 5 DMF molecules in a unit cell or 20 H_2O molecules in a unit cell. Figure 4c shows the effect of solvents in the pores on CO_2 adsorption in the 2-fold interwoven structure. As shown in this figure, the solvents in the pores do not give any remarkable influence on the gravimetric CO_2 adsorption, i.e., the increase in adsorption is canceled by the additional weight from the solvents. Therefore, the lower CO_2 adsorption for **1-S** than in the 2-fold interwoven structure at higher pressures in Figure 4a cannot be explained by guest solvents remaining in the pores. Hence, it seems that the low adsorption for the experimental samples (**1-C** and **1-S**) must result from the partial collapse of the framework and/or intraparticle mesopores during the evacuation. Here, partial framework collapse refers to the closing down of some portions of pores, especially large pores. Similarly, collapse of mesopores between particles can prevent access to micropores by blocking the pores at particle/particle interfaces.[18]

4.3. Effects of Evacuation Methods on Adsorption of Other Gases. To generalize these results, we performed similar comparisons for adsorption of several gases at room temperature. Figures 5a, 5b, 5c, and 5d show the experimental and simulated isotherms of H_2, CO_2, CH_4, and C_2H_6 at 298 K. For each gas, the experimental isotherms for **1-C** and **1-S** are compared with the simulated isotherms for the original IRMOF-16 and the hypothetical 2-fold interwoven structures. As was the case with the N_2 isotherm at 77 K, **1-S** exhibits much larger adsorption than **1-C** for all gases. The isotherms for **1-C** show weaker adsorption than the simulated isotherms for IRMOF-16 throughout the entire pressure range. The isotherms for **1-S** show stronger adsorption than the simulated isotherms of IRMOF-16 at low pressures but considerably lower adsorption at saturated regimes. For all gases except H_2, the crossovers between the isotherm for **1-S** and the simulated IRMOF-16 isotherm are observed within the chosen pressure range (0−20 atm). The H_2 isotherms do not show the crossover because the pressure range shown in Figure 5a is far from the saturated regime. In Figure 4, we see that the experimental CO_2 isotherm for **1-S** matches well with the simulated isotherm for 2-fold interwoven structure at low pressures. Here, we see that the same results are observed for H_2, CH_4, and C_2H_6.

Some of the simulated isotherms in Figure 5 show an inflection (S-shape). These "S-shaped" isotherms were already observed experimentally for several large-pore MOFs. Recently, Walton et al. were able to predict such

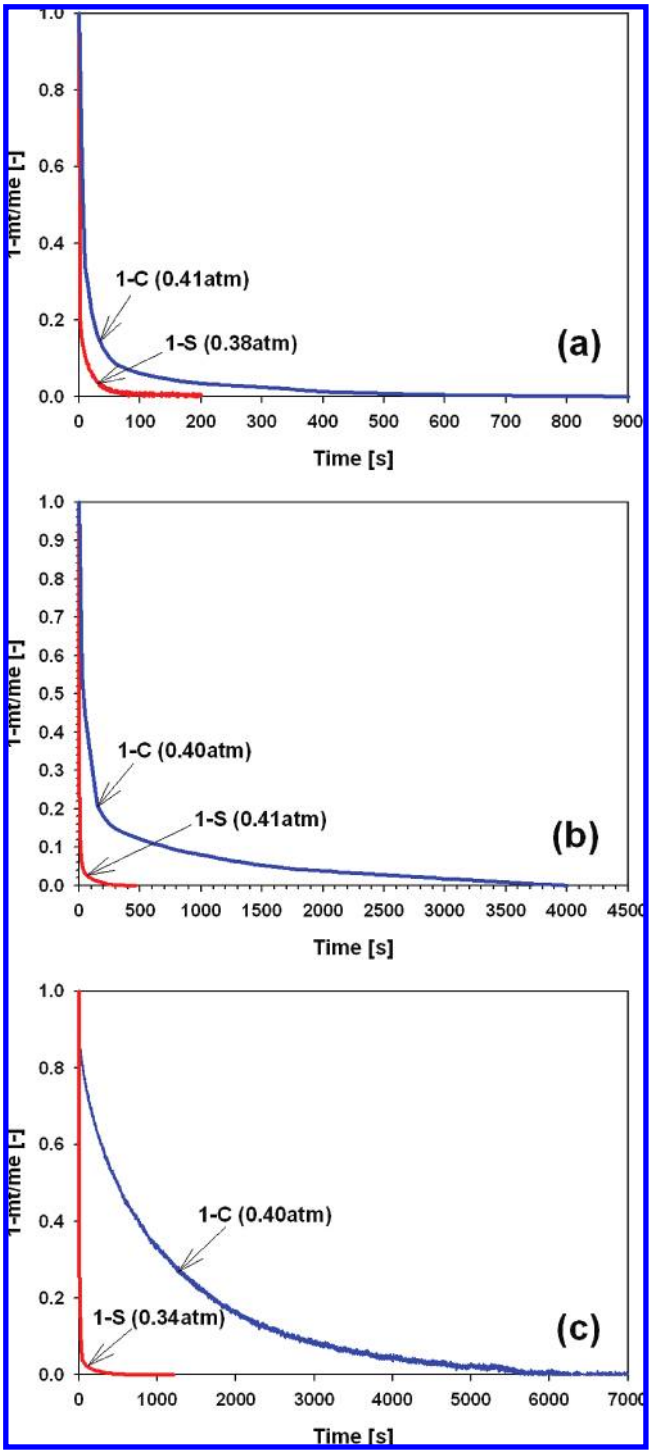

Figure 6. Comparisons of adsorption rates in **1-C** and **1-S** (at the first adsorption points): (a) CO_2, (b) CH_4, and (c) C_2H_6. In the figures, m_t is the amount adsorbed at a given time, and m_e indicates the amount adsorbed at equilibrium.

isotherms with GCMC simulations in excellent agreement with experiment. They found that the inflections come from attractive interactions between CO_2 molecules.[42]

Figure 6 compares the adsorption rates of CO_2, CH_4, and C_2H_6 on **1-C** and **1-S** at 298 K. All of the pressure uptake curves were obtained at the first point of each gas

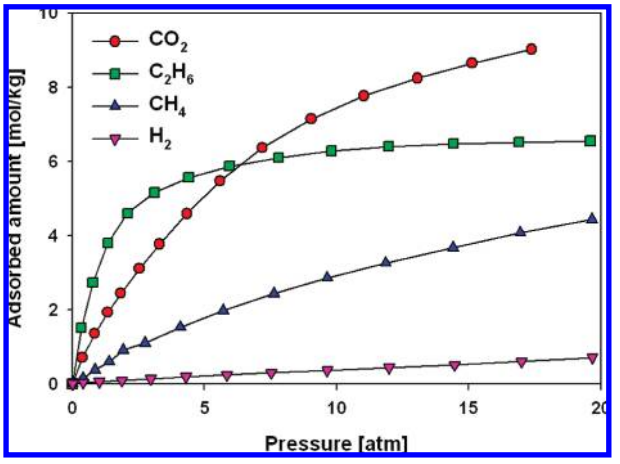

Figure 7. Comparison of four experimental gas adsorption isotherms in **1-S** at 298 K.

isotherm. From the N_2 isotherms at 77 K, we have already shown that both evacuated samples have similar pore size distributions, even though the pore volumes are considerably smaller for **1-C**. However, Figures 6a−c indicate that the adsorption rate of each gas is much slower in **1-C**. Moreover, although the adsorption rates of CO_2, CH_4, and C_2H_6 on **1-S** are very similar with each other, those on **1-C** can be correlated with the kinetic diameter of the gas molecules: CO_2 (3.3 Å) > CH_4 (3.8 Å) > C_2H_6 (4.0 Å) The slow adsorption in **1-C** may originate from some kinetic resistances on the exterior surface of the crystals. From these and previous results, we can conclude that the SCD evacuation is superior to the conventional $CHCl_3$ evacuation in view points of the adsorption kinetics as well as the adsorption capacity.

A comparison of the four gas isotherms in **1-S** at 298 K (Figure 7) illustrates considerably high adsorption selectivity of CO_2, CH_4, or C_2H_6 over H_2 as well as high adsorption capacities. This result indicates that **1-S** may be a good candidate for the production of hydrogen from coke oven gases (COGs),[43] which include ~50% H_2.

5. Conclusions

A large-pore isoreticular metal-organic framework (IRMOF) compound (IRMOF-16-like material, denoted hereafter as **1**) was synthesized solvothermally using *N*,*N*′-dimethylformamide (DMF) as the solvent. The as-synthesized sample (**1**) was evacuated by two solvent removal procedures: the original $CHCl_3$ exchange and the new supercritical carbon dioxide (SCD) method. Using combined experimental characterization and geometrical calculations including thermogravimetric analysis (TGA), powder X-ray diffractometry (PXRD), and pore size analysis, we suggest that **1** is a mixture of the non-interpenetrated IRMOF-16 and corresponding 2-fold interwoven structures. However, the surface area, the pore volume, and the gas adsorption at 298 K for the evacuated samples (denoted as **1-C** and **1-S**) were still considerably smaller than those of the proposed 2-fold

(42) Walton, K. S.; Millward, A. R.; Dubbeldam, D.; Frost, H.; Low, J. J.; Yaghi, O. M.; Snurr, R. Q. *J. Am. Chem. Soc.* **2008**, *130*, 406.

(43) Yang, J.; Lee, C. H. *AIChE J.* **1998**, *44*, 1325.

interwoven structure. We tried to explain these discrepancies by guest solvents remaining in the pores based on TGA results, but grand canonical Monte Carlo (GCMC) simulations for CO_2 adsorption showed that the solvents in the pores do not give any remarkable influence on the gas adsorption at solvent loadings consistent with TGA. Therefore, these discrepancies can be reasonably explained by a partial collapse of **1**, especially the large pores, during the evacuation by $CHCl_3$ and SCD methods. This argument is supported by the comparisons of experimentally measured pore size distributions with geometrically calculated ones. In addition, as briefly discussed elsewhere, prevention of the reversible collapse of interparticle mesopores seems to be important.[18] All of the gas adsorption results measured at 77 and 298 K showed that the new SCD evacuation considerably enhances the gas adsorption ability, compared to the conventional $CHCl_3$ evacuation. Moreover, from the comparisons of adsorption rates, we found that the SCD evacuation is superior to the conventional $CHCl_3$ evacuation from the viewpoint of the adsorption kinetics as well as the adsorption equilibria. In this work, we demonstrated a new method that combines several experimental methods and geometric calculations as well as GCMC simulations for the characterization of metal-organic frameworks (MOFs), especially large-pore ones. This should be helpful for future studies on the characterization of new MOFs possibly including some imperfectness in the crystalline phase, such as catenation and partial collapse.

Acknowledgment. This work was supported by the Korea Research Foundation Grant funded by the Korean Government (MOEHRD) (KRF-2006-352-D00040), the U.S. Dept. of Energy's Office of Science (Grant No. DE-FG02-01ER15244), the U.S. National Science Foundation (CTS-0507013), and by TeraGrid computing facilities. Acknowledgment is also made to the Donors of the American Chemical Society Petroleum Research Fund for partial support of this research.

Supporting Information Available: Adsorption measurement details. Potential parameters for GCMC simulations. Pore size distributions. Catenated MOF structures. This material is available free of charge via Internet at http://pubs.acs.org.